



● *Original Contribution*

A 3-D-PRINTED PATIENT-SPECIFIC ULTRASOUND PHANTOM FOR FAST SCAN

LIDIA AL-ZOGBI,^{*2} BRIAN BOCK,^{†,2} SAUL SCHAFFER,[‡] THORSTEN FLEITER,[§] and AXEL KRIEGER^{*}

^{*} Department of Mechanical Engineering, Johns Hopkins University, Baltimore, Maryland, USA; [†] Department of Mechanical Engineering, University of Maryland, College Park, Maryland, USA; [‡] Department of Mechanical Engineering, Carnegie Mellon University, Pittsburgh, Pennsylvania, USA; and [§] R. Cowley Shock Trauma Center, Department of Diagnostic Radiology, School of Medicine, University of Maryland, Baltimore, Maryland, USA

(Received 17 August 2020; revised 2 November 2020; in final from 3 November 2020)

Abstract—Ultrasound phantoms are commonly used to assess the performance of ultrasound systems and ensure their proper functionality, in addition to providing opportunities for medical training. However, Focused Assessment with Sonography for Trauma (FAST) phantoms, in particular, are prohibitively expensive and procedure specific. This work explores the use of additive manufacturing to fabricate a patient-specific, full-scale torso ultrasound phantom. Phantom geometry was derived from anonymized computed tomography scans and segmented into discrete organs. The digital organs (torso, skeleton, liver, spleen) were 3-D printed and used as castable molds for producing their respective body features. These organs were integrated with artificial hemorrhages to produce a realistic training tool for FAST scans. The resulting phantom is low in cost, has a verified shelf-life of at least 1 y and was positively reviewed by a trauma and emergency radiologist for its ability to provide accurate geometric and ultrasound information. (E-mail: lalzogb1@jh.edu) © 2020 World Federation for Ultrasound in Medicine & Biology. All rights reserved.

Key Words: Ultrasound phantom, 3-D printing, Focused Assessment with Sonography for Trauma scan, Patient specific.

INTRODUCTION

Ultrasound phantoms are widely used for calibration of ultrasound equipment to ensure proper functionality (Culjat et al. 2010) and for medical training. Medical training includes procedures such as venous cannulation (Kendall and Faragher 2007; Morrow and Broder 2014), surgical planning (Wang et al. 2017; Garcia et al. 2018) and Focused Assessment with Sonography for Trauma (FAST) scanning (Kendall and Faragher 2007; Wells and Goldstein 2017). Commercially available medical phantoms made by companies such as CAE Healthcare (Sarasota, FL, USA), CIRS (Norfolk, VA, USA) and Kyoto Kagaku (Kyoto, Japan) provide stable products constructed from tissue-mimicking materials (TMMs); however, these products are often procedure specific, meaning that different phantoms would need to be purchased for training in different ultrasound practices. In conjunction with their high

cost, such phantoms are thus unaffordable for institutions with limited resources and can become insufficient for training larger groups (Tanius et al. 2015). Low-cost alternatives have been documented in the literature and can be broken down into two broad categories; the first category consists of phantoms that are composed of organic materials, such as gelatin, Metamucil (Luchs et al. 2007), chicken breasts, pig hearts (Culjat et al. 2010) and grapes (Fornage 1989). Though these materials are more affordable and readily available, their organic nature makes them vulnerable to decay within a week (Aoyagi and Hiraguri 2017), rendering them impractical for long-term use. To mitigate this problem, the second category of phantoms was developed, whereby inorganic materials were used as the main constituent. Materials such as sodium alginate (Aoyagi and Hiraguri 2017), poly(vinyl alcohol) (Surry et al. 2004), paraffin wax (Vieira et al. 2013), 3-D-printed photocurable materials (Bucking et al. 2017; Garcia et al. 2018) and ballistics gel (Morrow and Broder 2014; Morrow et al. 2016) have been explored with higher degrees of success, turning them into primary candidates for contemporary phantom production.

Address correspondence to: Lidia Al-Zogbi, Mechanical Engineering, Johns Hopkins University, Baltimore, MD 21218, USA. E-mail: lalzogb1@jh.edu

² Authors Lidia Al-Zogbi and Brian Bock contributed equally to this work.

To create patient-specific phantoms, many researchers have turned to 3-D printing modalities for their ability to reproduce complex geometries from patient imaging data with high fidelity at a relatively low cost. The process of creating such phantoms starts with collection of 3-D patient data from magnetic resonance imaging and/or computed tomography (CT) scans. The resultant scans are subsequently segmented into different organs using commercial software ([Eliceiri et al. 2012](#)), and a stereolithography file (STL) is generated to enable 3-D printing of the relevant anatomy. The work of [Filippou and Tsoumpas \(2018\)](#) provides an in-depth review of 3-D printing phantoms for numerous medical imaging modalities.

This article focuses on phantoms for FAST scanning, which is an ultrasound imaging technique used to identify significant hemorrhages in the peritoneal, pericardial and pleural spaces, as well as to identify pneumothoraces (lung collapse). It is one of the first and most crucial procedures conducted on incoming trauma patients. In the United States, the vast majority of FAST studies are performed at trauma centers by trauma surgeons and trainees, as well as emergency medicine physicians ([Moore et al. 2006](#); [Natarajan et al. 2010](#)). Though [Hazelaar et al. \(2018\)](#) created a patient-specific thorax phantom, silicone was employed as a TMM, which has inappropriate attenuation coefficient and speed of sound for ultrasound applications ([Robertson et al. 1992](#)). All aforementioned non-commercial phantoms are smaller-scale phantoms (<20 L, as opposed to ~30 L for an average male adult). Moreover, the literature does not contain any efforts to create a patient-specific FAST scan phantom, likely because of the complex logistics involved in designing, manufacturing, storing and transporting what would undoubtedly amount to a voluminous and weighty product. Additional complications can hinder attempts at creating such phantoms, such as the manufacturing and deposition of TMMs at larger volumes, whereby undesired bubble formation within cast viscous materials takes place. The contribution of this work lies in the development, implementation and validation of a method for producing life-sized, low-cost, patient-specific, mechano-acoustically valid ultrasound phantoms for FAST scan applications. The phantom was evaluated quantitatively and qualitatively by a trauma and emergency radiologist in categories including mechanical compliance, tactile realism, echographic verisimilitude and biorealism.

This article is organized into four sections: (i) Methods, including detailed information on design goals, image acquisition and segmentation procedures, material selection and the phantom production process; (b) Results, reporting the phantom's mechanical and acoustic properties, comparison of the final product with the

original design and the physician's assessment; (c) Discussion, providing an insightful analysis of the results and future work prospects, and finally (d) Conclusions, summarizing key elements of our work.

METHODS

Design goals and specifications

The design choices of the patient-specific ultrasound phantom were derived from the specifications required by users of the phantom. Combing through the literature and consulting expert radiologists, we identified five desirable parameters of an ultrasound phantom: (i) low cost; (ii) patient specificity; (iii) longevity and ease of storage; (iv) realistic haptic feedback; and (v) echographic realism.

For instance, a commercial FAST scan phantom can cost anywhere between US\$16,500 and US\$28,000, and the produced phantom should be at least half as expensive as US\$16,500. Patient specificity is identified in this article as the average geometric difference between the patient and the phantom, as measured by a CT scan. Longevity is qualitatively assessed by comparing the condition of the phantom moments after its creation with both its external and internal states after at least 6 mo. After this period, the phantom should be free of meaningful degradation, that is, defects that negatively affect its usability or realism. In addition, the phantom must be able to be stored under ambient conditions of temperature, humidity and pressure; any special storage requirements, particularly a freezer environment, would drastically reduce the phantom's practicality. The stiffness of the phantom's flesh (a component of its haptic feedback and mechanical properties) must be comparable to that of a human, as evaluated by a radiologist. Lastly, the materials selected for the tissues, organs and bones must have similar relative acoustic properties to those of their human counterparts to obtain realistic and analyzable scans. The overall development and manufacturing process is briefly described in [Figure 1](#).

Image acquisition and segmentation

The design of the phantom was based on an anonymized 36-y-old male patient. DICOM images from a CT scan of the patient with a pixel size of 1 mm were used to segment various organs using intensity thresholding, and STL files of the skeleton, liver, spleen and torso were subsequently obtained using the open-source software 3-D Slicer ([Fedorov et al. 2012](#)), as well as the commercial software Materialize Mimics (Materialize NV, Leuven, Belgium). The mesh modeling software Meshmixer (Autodesk, San Rafael, CA, USA) allowed us to manually correct inaccuracies and non-uniform organ segmentation in the STL files.

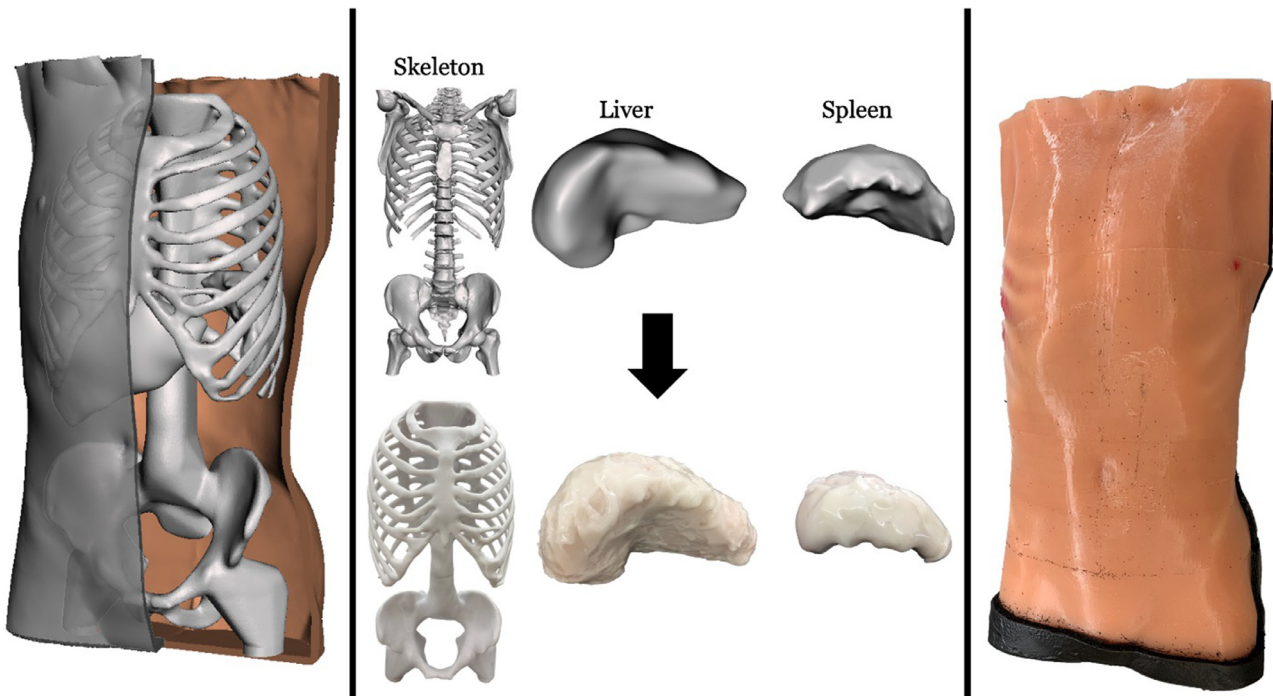


Fig. 1. Overview of the design and manufacture of the phantom. The digital organs (center, left) are derived from computed tomography scans, 3-D printed and used as molds to create the physical phantom components (center, right).

Material selection

Tissue simulant. The tissue simulant comprises the bulk flesh of the phantom torso, as well as the liver and spleen. The crucial properties, derived from the Design Goals and Specifications, guided the material selection process for the tissues: (i) castability for creating specific geometries; (ii) long-term stability at room temperature; (iii) realistic mechanical properties; and (iv) realistic ultrasound properties.

Humimic Medical (Greenville, SC, USA) and Clear Ballistics (Greenville, SC, USA) produce a variety of ballistic gels with realistic ultrasound properties and a range of mechanical properties, which can be melted and thus poured into a mold. The gels are stable at room temperature, are inorganic, and do not degrade over time, meeting the required criteria for our application.

A Shore OO durometer (Qingdao Realtech Instrument, Qingdao City, Shandong Province, China) was used to measure the Shore hardness on two men aged 22 and 43 to obtain a target hardness for the torso simulant material. A total of 12 different measurements were sampled from each participant, all from the umbilical and hypogastric regions to capture the tissues' hardness unaltered by skeletal presence. The body composition of the two patients closely matches that of the initial patient, and the average Shore hardness of all measurements amounted to 12.7.

Clear Ballistics' 10% Synthetic Ballistic Gelatin (hereafter referred to as CBG10 for brevity) was revealed

to be too stiff, with a Shore hardness of 26.2. To mitigate this, a soft material needed to be mixed with it. Humimic Gel No. 5 is a considerably softer material, the hardness of which was unfortunately difficult to reliably measure because of its tendency to crumble. Therefore, Gel No. 5 and CBG10 were melted and mixed in different ratios until a hybrid gel with human-matching Shore hardness was obtained. The final composition, 30% CBG10 and 70% No. 5 Gel by weight, produced material with a Shore hardness of 12.8. This hybrid gel was subsequently used as the primary tissue simulant for the bulk of the phantom.

The organs (liver and spleen) comprised two materials: CBG10 and “white simulant,” that is, 90% undyed CBG10 mixed with 10% talcum powder (Johnny B., Commerce, CA, USA) by weight. The bulk of the organs was composed of CBG10, which was then coated with the white simulant to make the organs’ borders more easily distinguishable from the rest of the flesh under ultrasound, thus yielding a more physiologically accurate phantom. The total simulant volume required for the torso was ~30.4 L.

Skeleton. The skeleton geometry is prohibitively complex for traditional machining techniques, such as subtractive manufacturing. The model's complexity necessitates that the skeleton be produced *via* additive manufacturing, that is, 3-D printing. Polylactic acid (PLA) is a thermoplastic commonly used for fused

deposition modeling (FDM) 3-D printing applications (Li et al. 2016); however, the simulant melts at $\sim 93^\circ\text{C}$ – 121°C , whereas the heat deflection temperature (HDT) of PLA is only 55°C (Tabi et al. 2016). To avoid dramatic deformation under the thermal load of molten simulant, it was necessary to select a 3-D printable material with a higher HDT than PLA. Other material considerations include requirements of material strength, rigidity, print volume and total cost. Among the available 3-D printing materials and technologies, polycarbonate (Polycarbonate Thermoplastic, Stratasys, Eden Prairie, MN, USA), FDM 3-D printed on a Stratasys Fortus 400 mc (Stratasys, Eden Prairie, MN, USA), was chosen as a suitable material and manufacturing method for this application. The HDT of polycarbonate is 126°C – 138°C (depending on the pressure), allowing the material to remain stable and structurally sound when heated by the molten simulant. Because Fortus 400 mc has a print volume of $355 \times 254 \times 254$ mm, the skeleton was printed in two sections.

Design and manufacture of the phantom

Skeleton. The extracted STL file of the skeleton was cleaned and refined to reduce the complexity of anatomic features that would not be probed with the ultrasound, such as the spine and pelvic posterior. This included the addition of vertical rib supports parallel to the spine to strengthen the rib cage for 3-D printing, and removal of the lower coccyx. The clavicle, scapula and all vertebrae above the first thoracic were also removed (Fig. 2b, 2d). The costal cartilage could not be completely segmented from the CT scan and, therefore, had to be manually reconstructed (Fig. 2b). The ball-socket degrees of freedom of the hips were disadvantageous to the standing stability of the phantom, so each femoral head was widened and fused with the pelvis. Cylindrical pins were modeled into the skeletal base and the torso mold base to ensure alignment between the two (Fig. 2e, 2f). Because of print volume constraints, the skeleton was bisected along the transverse plane just below the ribs and printed in two pieces. The two halves were mated with press-fit steel pins (52100 alloy steel, 10 mm in diameter, 100 mm long, McMaster-Carr, Elmhurst, IL, USA) embedded inside the spine (Fig. 3), further reinforced with SCIGRIP Weld-On 16 Cement (IPS Corp., Compton, CA, USA).

Liver and spleen. The liver and spleen were produced via casting methods. The liver was segmented from the CT scan and smoothed to reduce the model's complexity and eliminate features that would be difficult to cast, including narrow cavities and jagged edges (Fig. 4a, 4b). The smoothed liver model was hollowed

and bisected to conform to print volume constraints. The resulting model was FDM 3-D printed in PLA, assembled and used as a mold to cast the liver (Fig. 4c). To prevent it from melting, the mold was submerged in ice during pouring of the simulant. Before casting, the internal surfaces of the mold were coated with Henkel Loctite Frekote 770-NC (Henkel, Dusseldorf, Germany) to facilitate the separation of the organ. After cooling, the liver was extracted and dipped in the molten white simulant (Fig. 4d), as per the Material Selection Section for the Tissue Simulant. The process for producing the phantom spleen is almost identical to that for the liver, with the only difference being that the mold was designed for a toolless disassembly, favoring a bolted interface instead of an epoxied seam (Fig. 4f, 4j).

Torso. The torso was smoothed and then hollowed with 10-mm-thick walls (Fig. 5b). The top of the torso was left open to place the other body parts inside. The torso mold was FDM 3-D printed in PLA (ecoPLA, 3-DJAKE, Niceshops, Saaz, Austria) on a Delta Wasp 4070 Industrial (WASP, Massa Lombarda, RA, Italy) in three equal sections, split by transverse parallel planes (Fig. 5c). Although the torso is subject to the same thermal conditions during casting as the skeleton, it is not practical to print the torso in polycarbonate for three major reasons: (1) the size of the torso would have required a further compartmentalized multipart print (split along transverse and sagittal planes), complicating both print time and assembly; (2) the polycarbonate torso would have been significantly more costly than a PLA torso; and (3) because the torso mold needed to be cut off the phantom, it would have been more difficult to cut through polycarbonate than PLA. Additionally, unlike the skeleton structure, the torso can be submerged in ice, keeping it below its HDT despite the molten simulant inside. The three PLA torso sections were bonded together with SCIGRIP Weld-On 16 Cement, and then waterproofed with Flex Seal Spray (Flex Seal Spray Rubber Sealant Coating, Black, Swift Response, Weston, FL, USA) and Gaffer tape (Black, 2 in \times 30 yd, Gaffer Power, South Pasadena, FL, USA) (Fig. 5e). The waterproofing was necessary to ensure the quality of the final phantom, as the torso was cast fully submerged in ice. The internal surfaces of the torso mold were also coated with Henkel Loctite Frekote 770-NC.

Hemorrhages. The phantom contains three hemorrhages at anatomically correct locations. The two organ hemorrhages, affixed to the liver and spleen, respectively, consist each of a 91-cm latex balloon (Koogel, Koogel Store, Amazon) partially filled with 500 mL of water. Both organ hemorrhages were affixed to their organs via twine (string diameter 1 mm, two-ply jute

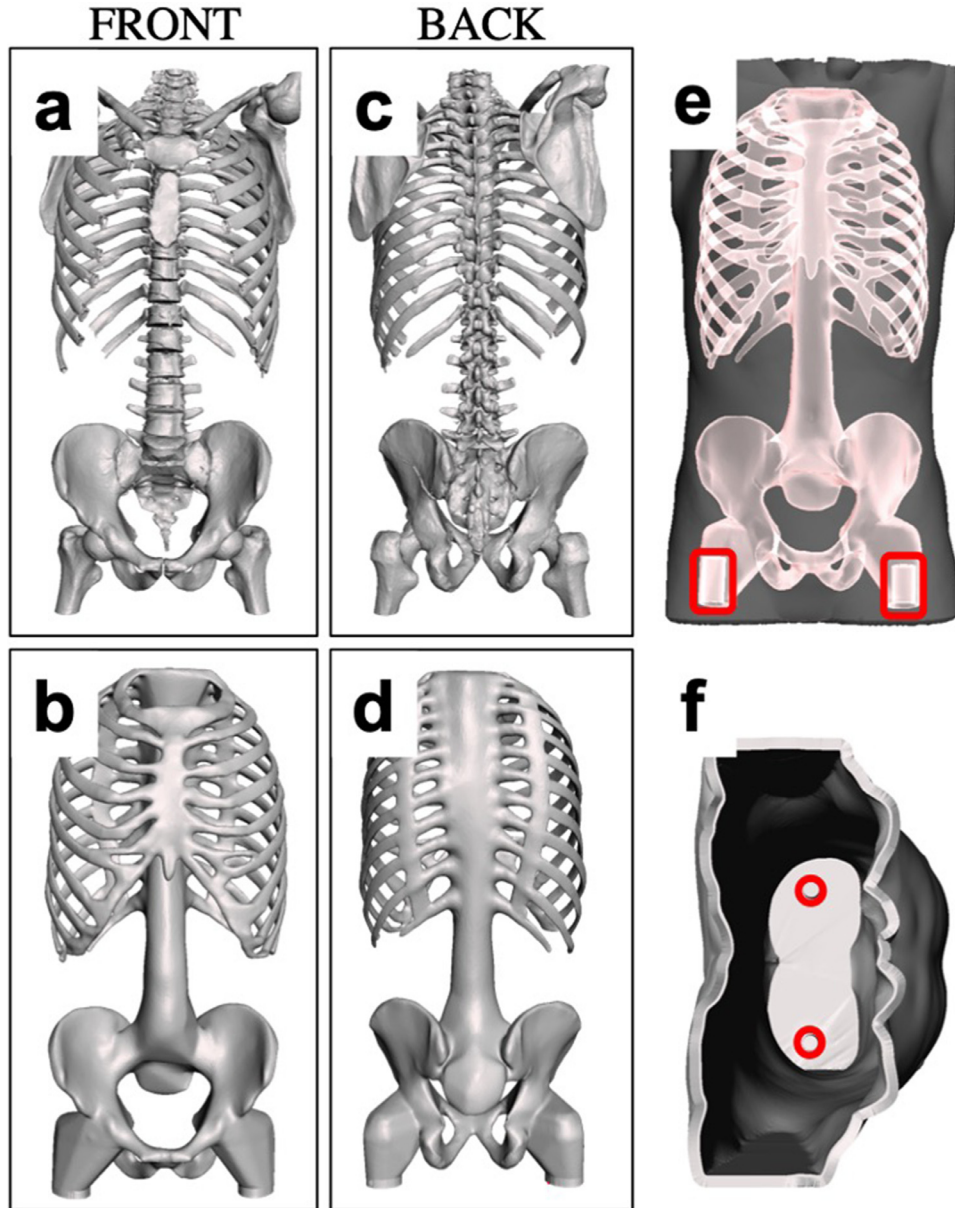


Fig. 2. (a) Front view of the original skeleton segmented from the computed tomography (CT) scan. (b) Matching view of the digital skeleton stereolithography file (STL) simplified for 3-D printing. (c) Rear view of the original skeleton segmented from the CT scan. (d) Matching view of the digital skeleton STL simplified for 3-D printing. (e) Front view of the skeleton superposed inside the torso with cylindrical alignment pins highlighted. (f) Top-down view of the torso mold with cylindrical alignment pins highlighted.

twine, Kinglake, Amazon) (Fig. 6a). The third, resting on the pelvic pubic symphysis, is a water balloon (Bunch O Balloons rapid-filling self-sealing water balloons, Zuru, Luohu District, Shenzhen, China) filled with 250 mL of water. This pelvic hemorrhage was suspended from the lower spinal column via twine (Fig. 6b).

Assembly. The assembly and casting process was conducted in the following order: (i) creation of organs, hemorrhages, skeleton and torso mold; (ii) affixation of

hemorrhages to organs; (iii) mounting of organs and hemorrhages on skeleton; (iv) assembly of skeleton inside the torso mold; (v) filling of torso mold with molten simulant; (vi) allowing phantom to cool; and (vii) cutting the torso mold off the phantom.

The liver and spleen were in turn suspended with their respective hemorrhages from the rib cage using twine (Fig. 7). The twine was wrapped around each organ and several ribs, secured in place with knots and SCIGRIP Weld-On 16 cement.

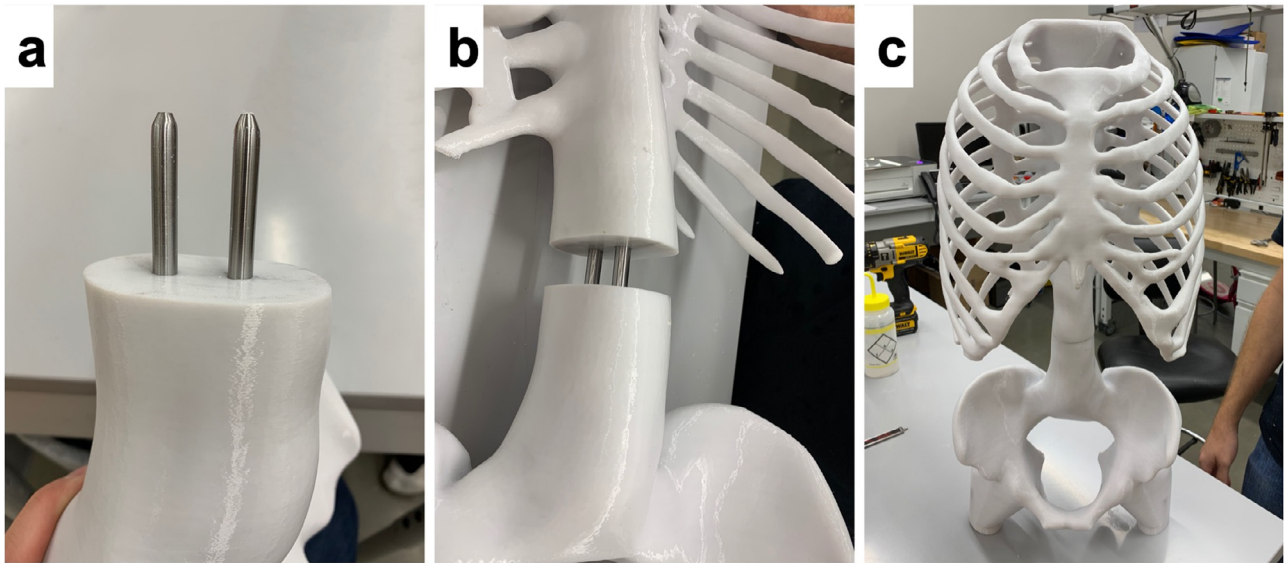


Fig. 3. Skeletal assembly. (a) Steel pins embedded in the pelvic side of the skeleton to mate the two halves. (b) Both halves of the skeleton mated with pins. (c) Fully assembled skeleton.

To promote cooling and mitigate possible thermal deformation, the phantom was cast with the torso fully submerged in ice. The geometry of the skeleton and its placement inside the torso dictated the order of assembly of the skeleton and torso thirds (Fig. 8a–d). A 121-L trash bin (Heavy Duty Trash/Garbage Can, 32 Gallon, Rubbermaid, Atlanta, GA, USA) was used as an ice reservoir for casting and required ~55 kg of crushed ice to fill.

The torso mold was sacrificial and used only for casting the torso, after which it was carefully cut off the phantom using an ultrasonic knife (H520 TCV55 K, Abbeon, Ventura, CA, USA). The torso mold was cut along the coronal and sagittal planes from the top downward, stopping 5 cm short of the base, and then cut circumferentially (parallel to the transverse plane) about

the front half of the mold (Fig. 8e). In this way, the base of the phantom was preserved as a rigid foundation for when the phantom is positioned upright, and the back was retained as one piece attached to the base to further improve stability and durability for transport and handling. The phantom posterior and base were not designed to be probed with ultrasound, so this additional support material does not alter the phantom's functionality.

RESULTS

Longevity and cost

The phantom has been stored as of December 2020 for 1 y 4 mo under ambient conditions, and transported multiple times in open air without any signs of

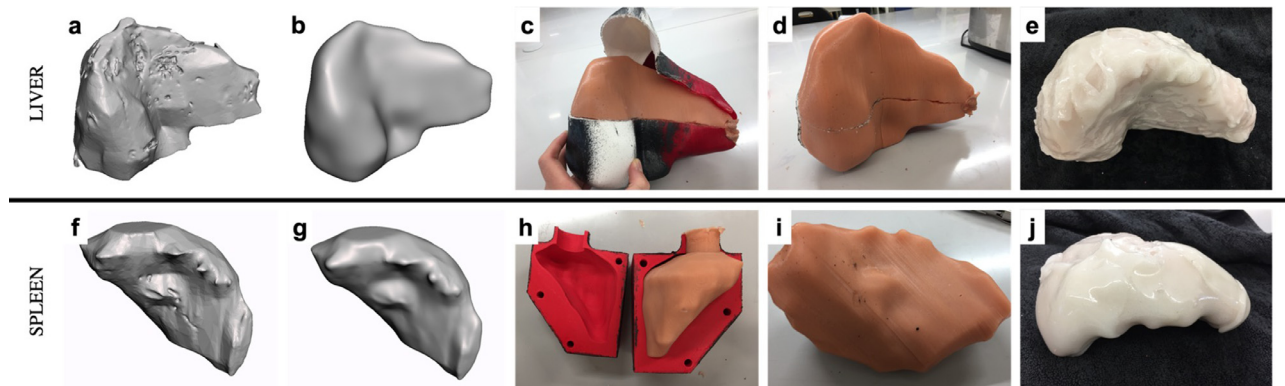


Fig. 4. (a) Digital view of the liver segmented from the computed tomography scan. (b) Matching view of the digital liver stereolithography file smoothed for 3-D printing. (c) CBG10 liver in mold. (d) Liver out of mold. (e) Completed liver coated in white simulant. (f) Digital view of the spleen segmented from the computed tomography scan. (g) Matching view of the digital spleen stereolithography file smoothed for 3-D printing. (h) CBG10 spleen in mold. (i) Spleen dipped in white simulant. (j) Completed phantom spleen.

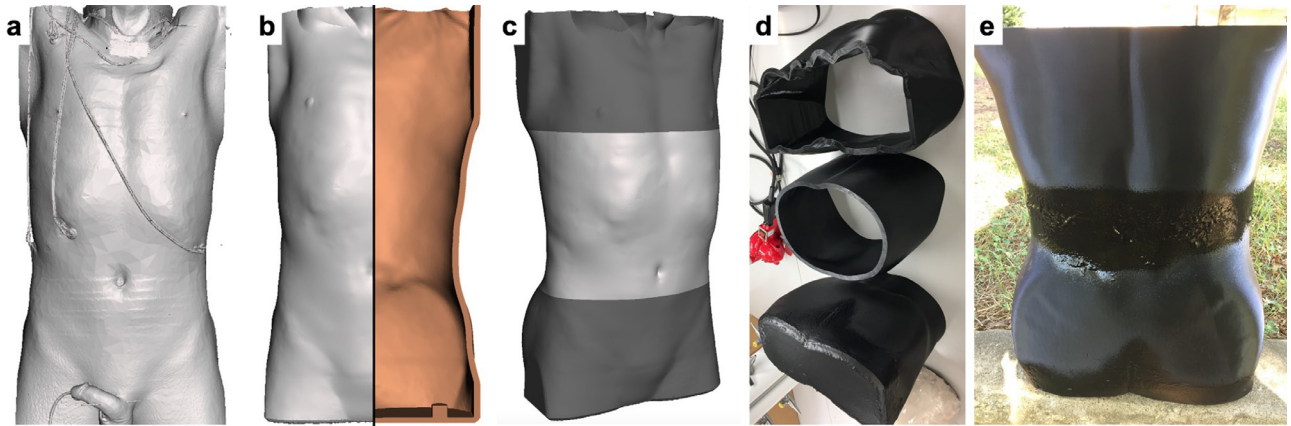


Fig. 5. (a) View of the original torso segmented from the computed tomography scan. (b) Matching view of the torso stereolithography file smoothed for 3-D printing with a partial cross-section (sagittal and coronal planes). (c) Digital view of the torso mold with the sectioned thirds shown. (d) The final three 3-D printed sections. (e) Lower and middle torso thirds adhered and sealed with flex seal.

degradation. Because of the closeness between some ribs and the torso, the tissue on one of these ribs moderately tore with handling, yet without affecting the phantom's functionality. The phantom is expected to last at least one additional year in good condition, except for minor wear and tear that could arise from usage.

The final phantom cost US\$2,160 to produce, including all manufacturing materials and 3-D printing costs. This is an order of magnitude less expensive than comparable commercially available models.

Adherence to the original design

To analyze the similarity between the designed phantom and the manufactured phantom, a CT scan of the physical phantom was obtained and subsequently segmented to extract STL and VTK files of the torso and

skeleton. The libpointmatcher library (Pomerleau *et al.* 2013) was used for finding the matching ratio of 3-D coordinate points between the designed and implemented phantoms using the iterative closest point algorithm (Besl and McKay 1992). The similarity of the torso's geometry was 98.3%, and that of the skeleton, 93.4%. The matching algorithm also returns a 4×4 transformation matrix, which allows to superimpose both geometries for performing additional comparative volumetric analyses using mesh nodes. The most common comparison metrics are intersection over union, Dice coefficient, false positive rate, false negative rate and the Dice and Hausdorff coefficients. The false positive rate metric represents the volume of the physical phantom that exceeds the designed volume (such as overflowing regions), whereas the false-negative rate represents the

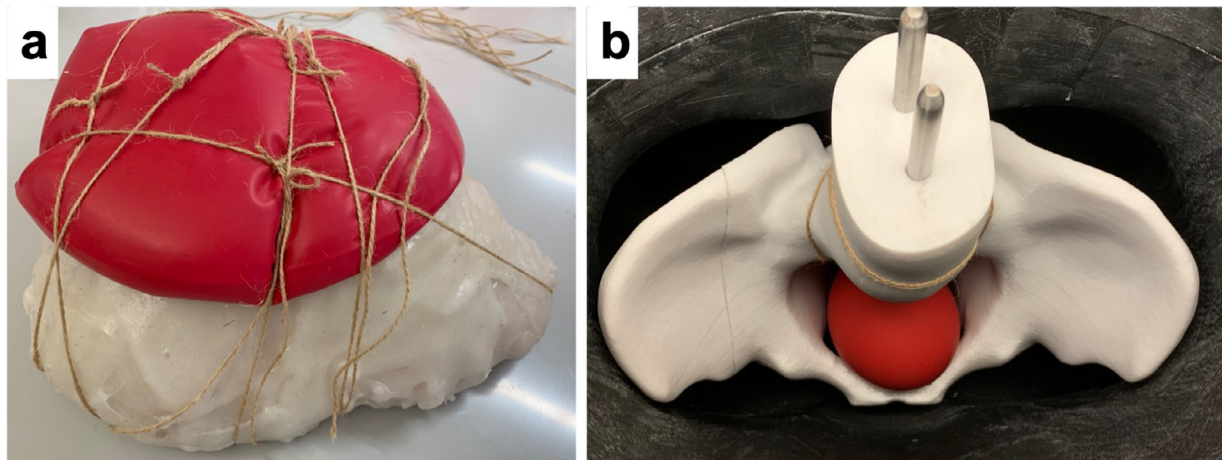


Fig. 6. (a) Liver hemorrhage affixed to the liver with twine. (b) Pelvic hemorrhage suspended from the lower spinal column.

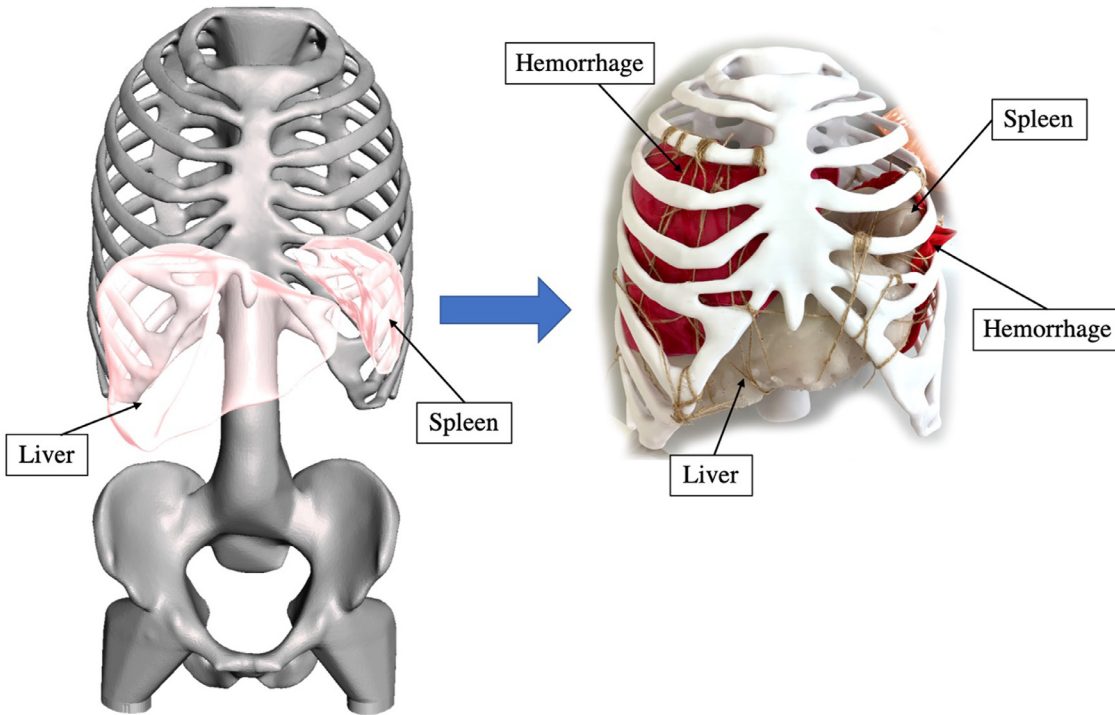


Fig. 7. Liver and spleen superposed in the skeleton model (left) and phantom organs affixed to physical rib cage (right).

volume that did not occupy the designed model (such as dents). The Hausdorff coefficient was computed using MeshLab (Cignoni et al. 2008), facilitated by the MeshLabXML Python scripting interface (3-DLIRIOUS, Arlington, TX, USA). The resultant values for the torso and skeleton are individually reported in Table 1.

Mechanical testing and simulations

Ultrasound probe force test. To analyze the variation of the phantom's abdomen stiffness at different locations, the displacement of an ultrasound probe was recorded for application of a 20-N force, the recommended maximal force in ultrasound imaging

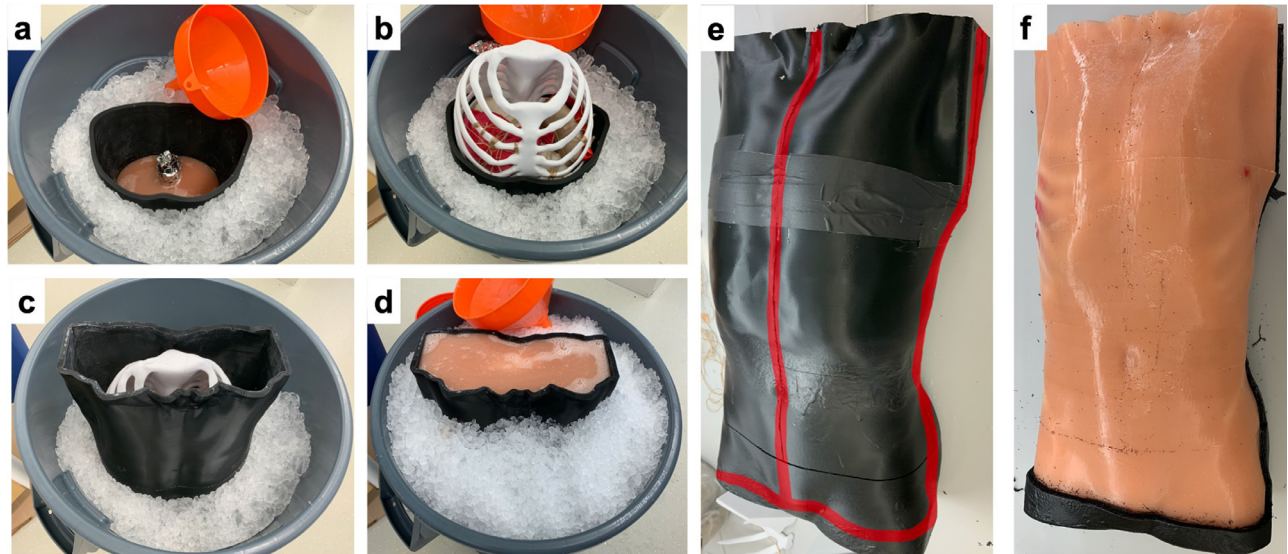


Fig. 8. (a) Lower third of the phantom cast. (b) Rib cage/organ assembly mounted on pelvis. (c) Top third of the torso mold in place. (d) Fully cast phantom. (e) Torso mold cut lines highlighted. (f) Torso mold fully removed.

Table 1. Volumetric comparison metrics between the designed and manufactured phantoms for the torso and skeleton components

| | Intersection over union | Dice coefficient | False positive rate | False negative rate | Hausdorff coefficient |
|----------|-------------------------|------------------|---------------------|---------------------|-----------------------|
| Torso | 98.3% | 99.1% | 2.4% | 0.2% | 0.98 mm |
| Skeleton | 93.4% | 96.6% | 6.3% | 2.3% | 2.10 mm |

(Fang et al. 2017). The test apparatus consists of an ultrasound probe (3.5 MHz Convex Probe, 2.0–5.0 MHz, CMS600 P2 Full Digital B-Ultrasound Diagnostic System, Contex Medical Systems, Hebei, China) affixed to an ATI Gamma Force/Torque sensor (ATI Industrial Automation, Apex, NC, USA), mounted on the end effector of a 7 DOF KUKA LBR iiwa (KUKA, Augsburg, Germany) (Fig. 9). To avoid measurement interference from the probe's cable, a full scale 3-D-printed mockup was used instead of the probe (shown in green in Fig. 9b). The ultrasound probe was robotically positioned mid-sternum on the phantom, and the 20-N force was applied axially in the robot's positive z-axis, with the resulting deflection into the body recorded. The displacement was measured from the moment the force sensor recorded an increase in sensed force, until 20 N was reached. Measuring the tissue displacement is a challenging task that would require special equipment, hence the probe's displacement computed from the robot's geometry and joints angles was instead considered for the same purpose.

The displacement profile was collected with the probe moving from the xiphoid to the umbilicus in 2.5-cm increments (Fig. 10a). The figure indicates a noticeable increase in displacement as the probe moves further away from the xiphoid, a profile that can be used for estimating the xiphoid's position based on force-displacement feedback. These measurements were subsequently used to validate mechanical simulations, which can provide opportunities for creating virtual phantoms from CT scans for other applications. Displacement-versus-force profiles have also been compared between the average of the two human patients used for estimating the Shore hardness of the tissues and the physical phantom, as illustrated in Figure 10b. It can be observed that the phantom underwent smaller deformations (indicating a stiffer body) than the average of the two human patients, particularly in the umbilicus region, which can be attributed to the absence of some internal organs in the phantom. However, the displacement at the xiphoid region was consistently smaller than that at the umbilicus

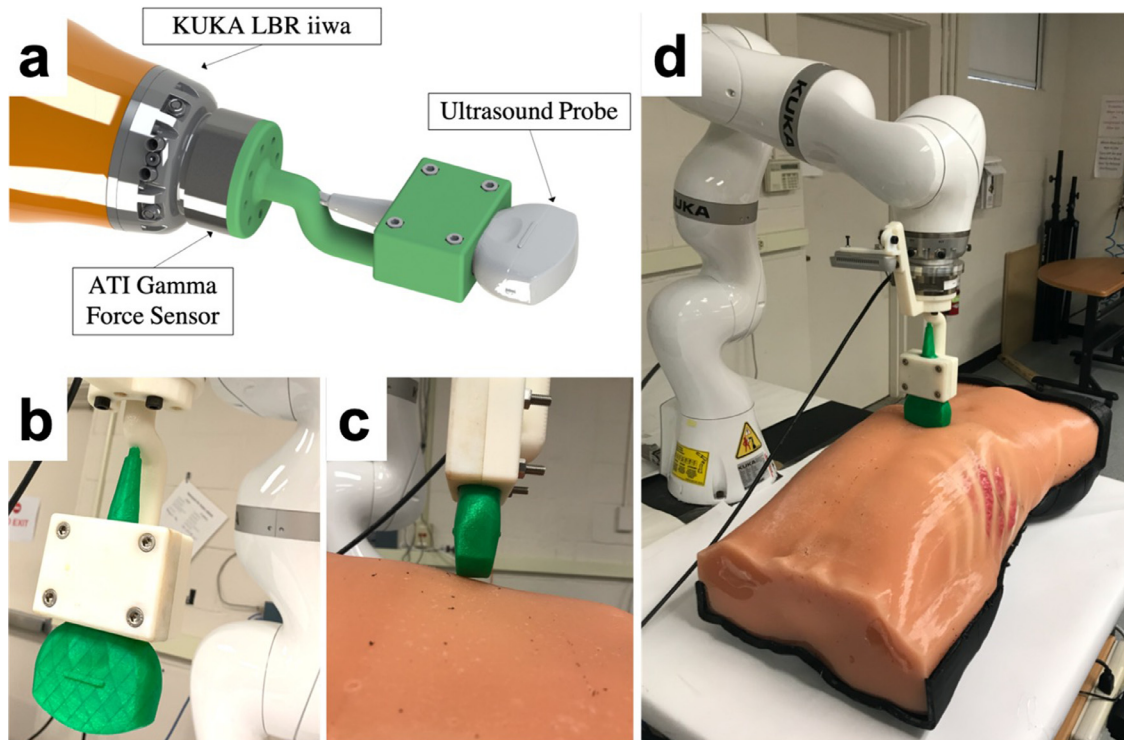


Fig. 9. (a) Rendering of probe/sensor. (b) Close-up photo of 3-D-printed ultrasound probe. (c) Close-up photo of the probe on the phantom just before applying force. (d) Photo of test with phantom.

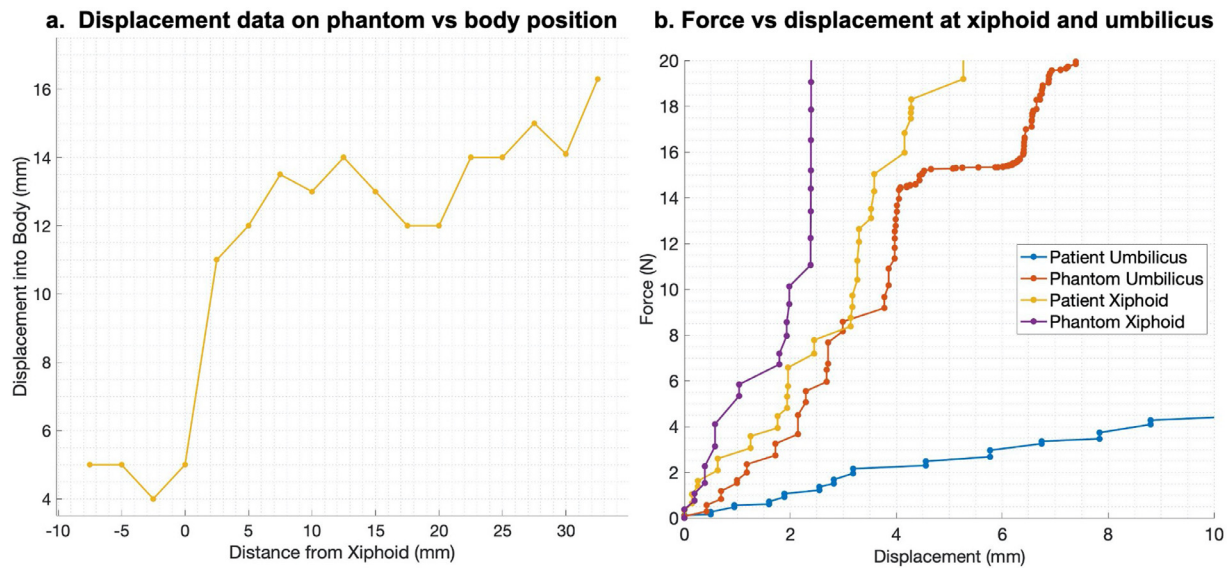


Fig. 10. (a) Probe displacement from a 20-N force application in 2.5-cm increments from the sternum to the umbilicus on the phantom using the robotic setup. (b) Force displacement data at the xiphoid and umbilicus regions of phantoms and patient. The xiphoid is considered the origin (zero point) for these data.

for the phantom, which aligns with the results observed in the average human patient.

Mechanical properties. Because the phantom tissue simulant is a thermoplastic elastomer, the Shore hardness determined using the durometer is not sufficient to mechanically characterize the material. A tensile stress test was thus performed using a mechanical testing device (Instron Model 5565, Instron Corp., Norwood, MA, USA), according to the ASTM D412 standard protocol (American Society for Testing and Materials [ASTM] 2006) under ambient temperature, humidity and pressure conditions. A dogbone-shaped aluminum mold was prepared for casting the test samples (Fig. 11). The melted tissue simulant is too viscous to allow for extraction of air bubbles using a vacuum chamber, hence the mold containing the simulant was placed on a heating plate (Isotemp Digital Hotplate 11-200-49 H, Thermo Fisher Scientific, Waltham, MA, USA) to facilitate the release of the bubbles, ensuring that the temperature does not exceed 250°F to avoid burning and hence damage of the simulant. The testing strain rate was set at 10 mm/s, and samples that failed at stress-concentrated regions (at the grips, or fillets) were discarded. A total of 30 samples were successfully tested, and the resulting stress-strain curves are provided in Figure 11c. The average Young's modulus was found to be 28.08 kPa with a standard deviation of 2.78 kPa, at a confidence level of 90%.

Finite element analysis. The mechanical tissue properties were then used as material inputs for ANSYS

(Canonsburg, PA, USA) finite-element analysis (FEA) simulations (Stolarski et al. 2018). The digital phantom is obtained from the CT scan performed on the phantom itself. The skeleton and tissue materials were segmented and converted from STL to IGS files, which are suitable for FEA computations. Similarly to the physical ultrasound probe force test, a 20-N force was applied through a probe on torso locations matching those of the robotic test. To ensure that the simulation replicates the settings of the actual test, a fixed holder was added to the probe to lock its motion in all directions but the z-axis (Fig. 12). The force was directly applied to the probe, using a varying load that gradually increased to 20 N over a period of 5 s. The probe was initially positioned at very close proximity to the torso; hence its total displacement was considered to be reflective of the tissue's displacement. Figure 12b illustrates a comparison between the displacements for the simulated and physical phantoms, whereby a similar profile is observed for both curves, with an absolute average offset error of 2.89 mm.

Acoustic testing. Acoustic properties of both CBG10 and the white simulant were measured using a US-Wave Ultrasound Waveform Generator/Receiver (Lecoeur Electronique, Chuelles, France) at the Johns Hopkins University MUSIIC Lab. The test consisted of pulsing the simulant with a 1-MHz wave through known material thicknesses and recording the received waveforms on the other side. A total of 100 tests for each thickness and 15 thicknesses for each material were recorded, at a sampling rate of 125 MHz. The time of flight of the sound wave was calculated by taking the

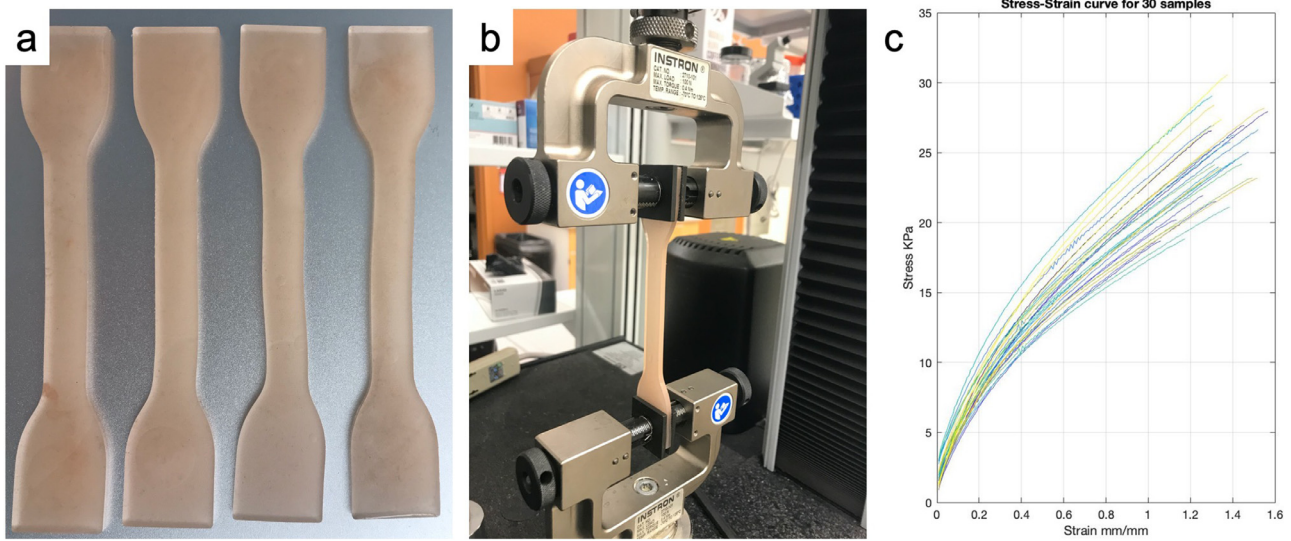


Fig. 11. (a) Dogbone-shaped specimens for tensile testing created via an aluminum mold. (b) The specimen in tensile testing using the Instron machine. (c) Resultant stress-strain curves of 30 specimens.

difference between the start of the non-zero distance waveform and the zero distance calibration waveform, which was then divided by the distance to yield the speed of sound. The speed of sound was then averaged over all of the thicknesses for each material, resulting in the final values of 1424 m/s for CBG10, and 1402 m/s for the white coating layer. The reported speed of sound of Gel No. 5 is 1466.00 m/s. Therefore assuming a linear interaction between the gel composition and the speed of sound, the phantom's tissue speed of sound becomes 1453.4 m/s. The average propagation speed of sound through human soft tissue is 1540 m/s (Christensen *et al.* 1978), which is comparable to the simulant's results.

Because of the restricted access to testing facilities amidst the coronavirus disease 2019 outbreak, this value had not been experimentally validated.

Physician assessment. The phantom was evaluated by an expert trauma and emergency radiologist involving a hands-on examination to explore the mechanical and tactile realism at specific regions (sternum, abdomen) and overall. The examination was immediately followed by an in-depth inspection of the phantom under ultrasound, evaluating specifically the four FAST scan locations (perihepatic space, perisplenic space, pericardium and pelvis) and the overall ultrasound appearance of the phantom simulant. It

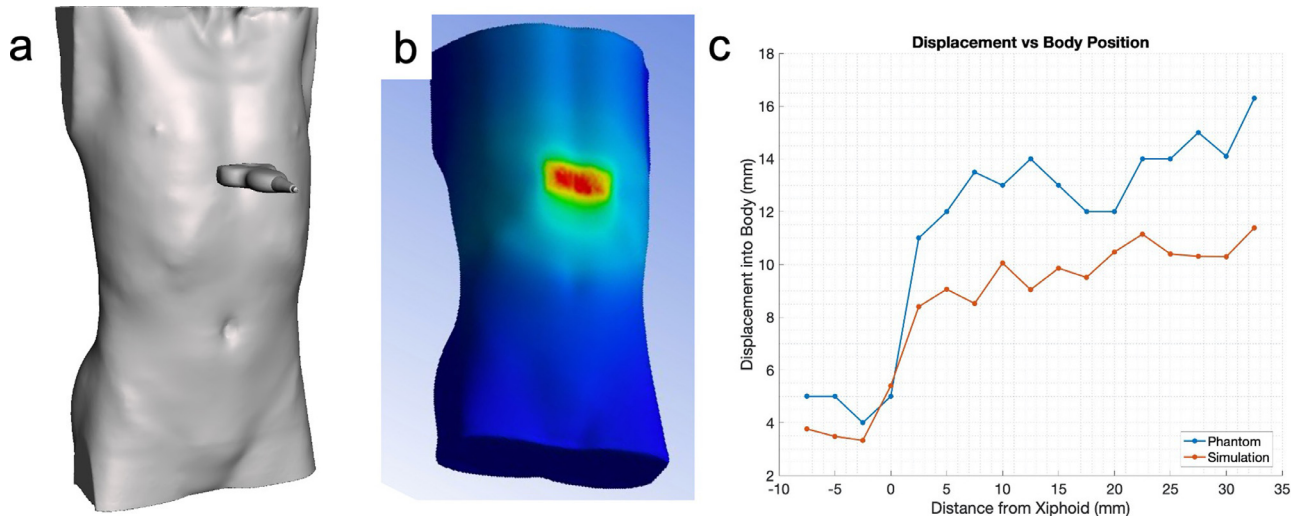


Fig. 12. (a) Overall problem setup for the finite-element analysis. (b) Resulting tissue displacement in ANSYS. (c) Comparison between simulated and measured probe displacements.

is important to evaluate each FAST scan location under multiple ultrasound views because some areas of interest could be harder to image, especially for trainees, such as the perisplenic space. The realism of the phantom in those specific regions becomes paramount and requires special attention from medical experts during the evaluation process. At the conclusion of the evaluation, the radiologist was interviewed for qualitative feedback on the phantom and then asked to complete a 25-question Likert scale evaluation spanning a wide variety of aspects of the phantom (reproduced in Appendix A, Supplementary Data, online only). On a Likert scale ranging from 1 (completely unrealistic) to 5 (comparable with other phantoms), the phantom received either a 4 or 5 on mechanical/tactile realism; size and placement of the liver and spleen; size of the perisplenic FAST scan location; size and location of the perihepatic FAST scan locations; ultrasound realism of the bulk flesh, liver and spleen; skeleton realism; and usefulness for training new FAST scan practitioners. The realism of the pelvic FAST scan location received a 2 for location and a 3 for size because of its nearly spherical shape and thin wall (balloon), which made it resemble a human bladder rather than a hemorrhage.

DISCUSSION

The phantom produced as described under Methods proved to be a viable ultrasound phantom for FAST scans. The final product adheres to the aforementioned design specifications and offers a more affordable solution for a wide span of applications, ranging from medical training to biomechanical simulations. Although the reported cost of the phantom is indeed lower than the cost of commercial phantoms, it does not, however, include labor and capital costs (*e.g.*, 3-D printers). The required technology, data and evaluation by at least one medical expert add extra layers of complexity that certainly leave room for future improvements. The phantom exhibited great similitude to the original design, highlighting the physiologic realism and patient-specific design that can be achieved using our proposed methodology. The phantom has preserved its shape, tactile feel and hemorrhages after 1 y 3 mo past its manufacture. Polycarbonate, as well as synthetic ballistic gelatin, are temperature-stable materials, which are not expected to degrade within the coming few years under ambient conditions. The hemorrhages, on the other hand, made of latex balloons rather than water balloons, have a more questionable durability. A better assessment of the longevity of the phantom should be obtained in the future by analyzing the shelf-life of individual components through a range of stress tests and subsequently reassessing mechanical properties of samples, and visually inspecting them for any signs of degradation.

Mechanical and acoustic testing was conducted to further characterize the phantom, and FEA simulations were used for digital modeling purposes. The FEA probe displacements displayed results comparable with those of the measured displacements, indicating that FEA can be used to simulate ultrasound phantoms for more virtual applications, such as training robotic systems using force-feedback. The usage of water as a substitute for blood, however, resulted in relatively low ultrasound contrast between the hemorrhages and tissue simulant, which makes the hemorrhages more difficult to discern. Blood has a 90 times larger ultrasound attenuation coefficient than water, which makes it appear nearly black under ultrasound scans. Further research will focus on determining a hemorrhage-mimicking fluid with better anechoic properties for improved contrast and visibility.

Future work will also explore the integration of additional organs or other internal complexities, as well as unconstrained hemorrhages for increased realism, utilizing injected free fluid instead of tethered balloons. Pericardial effusion, which is excess fluid between the heart and pericardium, should be incorporated into future phantom iterations, as it is routinely evaluated through FAST scanning. Phantoms will be developed and evaluated with the assistance of a larger body of physicians, comprising emergency medicine physicians and trauma surgeons, which would allow the creation of a phantom that can meet the needs of a larger medical community. Lastly, varying body habitus will be considered in future models because factors such as obesity can impose sonographic limitations, offering a necessary training environment for such challenging cases.

CONCLUSIONS

This article describes a methodology for creating a low-cost, patient-specific FAST scan phantom with realistic mechanical and acoustic properties that can be safely stored under ambient conditions of temperature, humidity and pressure. The phantom's geometry was obtained from anonymized CT scans, which were also used for generating the phantom's organs. The tissues were made of a combination of two different ballistic gelatin materials to achieve a human-like stiffness, cast into 3-D printed molds generated from the CT scans. The skeleton was 3-D printed out of polycarbonate, and the hemorrhages consisted of latex balloons partially filled with water. Mechanical and acoustic properties of the phantom were obtained, whereby tensile tests were performed, and the speed of sound across the tissue simulant was computed. The values were comparable to those reported for human tissues, and an expert trauma and emergency radiologist positively reviewed the phantom under ultrasound inspection.

Acknowledgments—The authors acknowledge and thank the following individuals, laboratories and organizations for their contributions: Abhishek Kathpal, University of Maryland, College Park, for assisting with the ultrasound probe force test; Megan Kemicata, University of Maryland, College Park, for providing guidance and assistance with the Instron machine at the Tissue Engineering & Biomaterials Lab, which was used to characterize the material properties of the phantom material; Terrapin Works and the Product Innovation & Realization Laboratory Suite, University of Maryland, College Park, for the use of their tools, facilities and 3-D printing capabilities; Dr. Emad Boctor and Yonsu Kim at the Medical UltraSound Imaging and Intervention Collaboration (MUSiiC) Research Laboratory, Johns Hopkins University, for acoustic testing of the phantom materials; and Clear Ballistics and Humimic Medical, for their product properties (density, Shore hardness and speed of sound).

Conflict of Interest—The authors declare that they have no conflict of interest.

SUPPLEMENTARY MATERIALS

Supplementary material associated with this article can be found in the online version at doi:[10.1016/j.ultra-smdbio.2020.11.004](https://doi.org/10.1016/j.ultra-smdbio.2020.11.004).

REFERENCES

- American Society for Testing and Materials (ASTM). Standard test methods for vulcanized rubber and thermoplastic elastomers-tension. ASTM D412-16. West Conshohocken, PA: Author; 2006.
- Aoyagi M, Hiraguri T. Ultrasound phantom using sodium alginate as a gelling agent. *J Ultrasound Med* 2017;36:2345–2353.
- Besl PJ, McKay ND. Method for registration of 3-D shapes. Sensor fusion IV: Control paradigms and data structures. Bellingham, WA: SPIE; 1992. p. 586–606 Vol. 1611.
- Bucking TM, Hill ER, Robertson JL, Maneas E, Plumb AA, Nikitichev DI. From medical imaging data to 3D printed anatomical models. *PLoS One* 2017;12(5) e0178540.
- Christensen EE, Curry TS, Dowd JE. An introduction to the physics of diagnostic radiology. Philadelphia: Lea & Febiger; 1978.
- Cignoni P, Callieri M, Corsini M, Dellepiane M, Ganovelli F, Ranzuglia G. Meshlab: An open-source mesh processing tool. Eurographics Italian chapter conference, Salerno, Italy. Geneva: Eurographics Association; 2008. p. 129–136. doi: [10.2312/Local-ChapterEvents/ItalChap/ItalianChapConf2008/129-136](https://doi.org/10.2312/Local-ChapterEvents/ItalChap/ItalianChapConf2008/129-136).
- Culjat MO, Goldenberg D, Tewari P, Singh RS. A review of tissue substitutes for ultrasound imaging. *Ultrasound Med Biol* 2010;36:861–873.
- Eliceiri KW, Berthold MR, Goldberg IG, Ibanez L, Manjunath BS, Martone ME, Murphy RF, Peng H, Plant AL, Roysam B, Stuurman N, Swedlow JR, Tomancak P, Carpenter AE. Biological imaging software tools. *Nat Methods* 2012;9:697–710.
- Fang TY, Zhang HK, Finocchi R, Taylor RH, Boctor EM. Force-assisted ultrasound imaging system through dual force sensing and admittance robot control. *Int J Comput Assist Radiol Surg* 2017;12:983–991.
- Fedorov A, Beichel R, Kalpathy-Cramer J, Finet J, Fillion-Robin JC, Pujol S, Bauer C, Jennings D, Fennessy F, Sonka M, Buatti J, Aylward S, Miller JV, Pieper S, Kikinis R. 3 D Slicer as an image computing platform for the quantitative imaging network. *Magn Reson Imaging* 2012;30:1323–1341.
- Filippou V, Tsoumpas C. Recent advances on the development of phantoms using 3 D printing for imaging with CT, MRI, PET, SPECT, and ultrasound. *Med Phys* 2018;45:e740–e760.
- Fornage BD. A simple phantom for training in ultrasound-guided needle biopsy using the freehand technique. *J Ultrasound Med* 1989;8:701–703.
- Garcia J, Yang Z, Mongrain R, Leask RL, Lachapelle K. 3 D printing materials and their use in medical education: A review of current technology and trends for the future. *BMJ Simul Technol Enhanc Learn* 2018;4:27–40.
- Hazelaar C, van Eijnatten M, Dahele M, Wolff J, Forouzanfar T, Slotman B, Verbakel WF. Using 3 D printing techniques to create an anthropomorphic thorax phantom for medical imaging purposes. *Med Phys* 2018;45:92–100.
- Kendall JL, Faragher JP. Ultrasound-guided central venous access: A homemade phantom for simulation. *CJEM* 2007;9:371–373.
- Li N, Li Y, Liu S. Rapid prototyping of continuous carbon fiber reinforced polylactic acid composites by 3 D printing. *J Mater Process Technol* 2016;238:218–225.
- Luchs JS, Sofka CM, Adler RS. Sonographic contrast effect of combined steroid and anesthetic injections: In vitro analysis. *J Ultrasound Med* 2007;26:227–231.
- Moore CL, Molina AA, Lin H. Ultrasonography in community emergency departments in the United States: Access to ultrasonography performed by consultants and status of emergency physician-performed ultrasonography. *Ann Emerg Med* 2006;47:147–153.
- Morrow DS, Broder J. Cost-effective, reusable, leak-resistant ultrasound-guided vascular access trainer. *J Emerg Med* 2014;49:313–317.
- Morrow DS, Cupp JA, Broder JS. Versatile, reusable, and inexpensive ultrasound phantom procedural trainers. *J Ultrasound Med* 2016;35:831–841.
- Natarajan B, Gupta PK, Cemaj S, Sorensen M, Hatzoudis GI, Forse RA. Fast scan: Is it worth doing in hemodynamically stable blunt trauma patients?. *Surgery* 2010;148:695–701.
- Pomerleau F, Colas F, Siegwart R, Magnenat S. Comparing ICP variants on real-world data sets. *Autonomous Robots* 2013;34:133–148.
- Robertson J, Leen E, Goldberg JA, Angerson WJ, Sutherland GR, McArdle CS. Flow measurement using duplex Doppler ultrasound: Haemodynamic changes in patients with colorectal liver metastases. *Clin Phys Physiol Meas* 1992;13:299–310.
- Stolarski T, Nakasone Y, Yoshimoto S. Engineering analysis with ANSYS software. Burlington, MA: Elsevier Butterworth-Heinemann; 2018.
- Surry KJM, Austin HJB, Fenster A, Peters TM. Poly(vinyl alcohol) cryogel phantoms for use in ultrasound and MR imaging. *Phys Med Biol* 2004;49:5529–5546.
- Tabi T, Hajba S, Kovacs J. Effect of crystalline forms (α' ; and α) of poly(lactic acid) on its mechanical, thermo-mechanical, heat deflection temperature and creep properties. *Eur Polymer J* 2016;82:232–243.
- Tanious SF, Cline J, Cavin J, Davidson N, Coleman JK, Goodmurphy CW. Shooting with sound: Optimizing an affordable ballistic gelatin recipe in a graded ultrasound phantom education program. *J Ultrasound Med* 2015;34:1011–1018.
- Vieira SL, Pavan TZ, Junior JE, Carneiro AA. Paraffin-gel tissue-mimicking material for ultrasound-guided needle biopsy phantom. *Ultrasound Med Biol* 2013;39:2477–2484.
- Wang K, Ho CC, Zhang C, Wang B. A review on the 3 D printing of functional structures for medical phantoms and regenerated tissue and organ applications. *Engineering* 2017;3:653–662.
- Wells M, Goldstein L. The role of phantoms and simulation in teaching ultrasound skills in emergency medicine. In: Connolly JA, Dean AJ, Hoffman B, Jarman, (eds). Emergency point-of-care ultrasound. 2nd ed. New York: Wiley; 2017.